Electrochimica Acta 474 (2024) 143538

Contents lists available at ScienceDirect

Electrochimica Acta

journal homepage: www.journals.elsevier.com/electrochimica-acta

Novel dynamic method based on CV-SECM and SWV-SECM for the in situ chemical imaging of reactive metal surfaces undergoing corrosion and corrosion inhibition illustrated with the case of copper corrosion inhibition by benzotriazole

B. Hernández-Concepción [a,+], R.M. Souto [a,b], J. Izquierdo [a,b,*]

[a] Department of Chemistry, Universidad de La Laguna, P.O. Box 456, E-38200 La Laguna (Tenerife), Canary Islands, Spain
[b] Institute of Material Science and Nanotechnology, Universidad de La Laguna, P.O. Box 456, E-38200 La Laguna (Tenerife), Canary Islands, Spain

ARTICLE INFO

Keywords:
Scanning electrochemical microscopy
Copper
Benzotriazole
Corrosion inhibition
Voltammetry
Gold microelectrode
Copper deposition
Anodic stripping

ABSTRACT

A novel dynamic method for the chemical imaging of actively corroding metal surfaces using scanning electrochemical microscopy (SECM) is proposed by using CV-SECM and SWV-SECM. This consists of an adequate coupling of a repetitive voltammetric operation at the SECM tip while conducting the rastering routine for scanning a reactive copper surface, as well as its inhibition by benzotriazole. In this method, gold microelectrodes are employed as SECM tips, and therefore their electrochemical behaviour towards collection and redissolution of Cu^{2+} ions from synthetic solutions containing Cu^{2+} ions. Next, the dynamic application of voltammetric methods for the collection and stripping of copper on the Au probes while mapping copper surfaces was investigated. The proof of concept first involved continuous cyclic voltammetry (CV-SECM) in an acidified NaCl solution, in terms of Cu^{2+} dissolution and surface redox activity (with SECM in the feedback mode). Then, square wave voltammetry (SWV-SECM) was used to detect small copper dissolution from corroding and inhibitor-protected metal surfaces. The results are consistent with a heterogeneous nature of copper degradation and the development of protective films and passive layers.

1. Introduction

Since the invention of scanning electrochemical microscopy (SECM), which uses microelectrodes as probes to detect electrochemical reactivity at metal/electrolyte interfaces [1,2], remarkable advances have been made in the science of corrosion [3] by providing images of local electrochemical reactivities on reactive surfaces which greatly contribute to the resolution of the ongoing mechanisms [3,4]. In this process, exploitation of the wide variety of operation modes available in the technique should be crucial. However, SECM has mainly been applied in corrosion systems using the traditional feedback mode, even though the conversion of redox mediators in the probe can significantly change the spontaneous mixed potential state of the freely corroding system [5]. The application of other amperometric modes such as substrate generation-tip collection (SG-TC) and redox competition (RC-SECM) have increased the versatility of the technique for the characterization of various forms of corrosion and protection phenomena which are reviewed elsewhere [3,6].

Interestingly enough, the application of operations modes other than feedback for the study of the effect of chemical corrosion inhibitors on the protection of metals has still been little explored. In fact, since the first investigations of Kontturi and coworkers [7–9] and Izquierdo et al. [10,11] in the inhibition of copper corrosion, all subsequent research for the screening of new inhibitor systems and their adsorption kinetics [12] are based exclusively on the feedback mode, that implies the addition of a redox mediator to the test electrolyte. As enlightening as it may be in revealing surface properties, this strategy would preferably be complemented by chemically resolving the species involved in heterogeneous surface reactions, using at least SG-TC to discern the local release of metal cations from the anodic active sites in order to address the achieved protectiveness. Only recently has our group explored the complementary use of SECM amperometric modes to image local

* Corresponding author at: Department of Chemistry, Universidad de La Laguna, P.O. Box 456, E-38200 La Laguna, Tenerife, Canary Islands, Spain.
E-mail address: jizquier@ull.edu.es (J. Izquierdo).
+ CIDETEC, Basque Research and Technology Alliance (BRTA), Paseo Miramón 196, 20,014 Donostia-San Sebastián, Spain

https://doi.org/10.1016/j.electacta.2023.143538
Received 31 October 2022; Received in revised form 15 November 2023; Accepted 19 November 2023
Available online 20 November 2023
0013-4686/© 2023 The Authors. Published by Elsevier Ltd. This is an open access article under the CC BY-NC-ND license (http://creativecommons.org/licenses/by-nc-nd/4.0/).

cathodic activity when studying a corroding galvanic couple model system subjected to chemical inhibition [13].

Concerning the local determination of metal cations, mercury-modified microelectrodes have proven to be very efficient for the local detection of species whose amperometric determination is not straightforward with conventional microdisc electrodes. Particular attention has been paid to alkali metals involved in energy storage [14,15], the release of Zn from corroding surfaces [16,17] or ZnSe waveguides [18], amongst other species from inorganic materials [19] and soil [20], the latter including copper(II). All these studies share the need to modify the microdisc electrode with a toxic element (mercury), thus generating a highly selective electroanalytical tool at the expense of complexity. Alternatively, the potentiometric mode of SECM and the scanning ion electrode technique (SIET) have emerged in recent years as promising alternatives for the selective determination of those ions using microsensors based on ionophore cocktails for the potentiometric characterization of materials [21–24], also implementing the potentiometric determination of Cu^{2+} [25].

Regarding copper corrosion inhibitor systems, the desired detection of aqueous copper ions using mercury-free electrodes has been attempted using under- or over-potential deposition (UPD and OPD, respectively) on (micro-) gold electrodes, followed by an anodic stripping process [26,27], a procedure recently implemented in a carbon-based microelectrode as well [28]. This electroanalytical procedure has also been implemented in SECM [29,30] and AFM-SECM [31,32] under potentiostatic conditions, although it required subsequent anodic stripping of the deposited copper from the tip at the end of a line scan, an operation which is performed after retrieval of the tip from the proximity of the investigated sample to be placed in the bulk of the solution. However, unavoidable fouling of the probe would immediately alter the actual response of the sensor while the scan is in progress. The continued removal of deposited copper during the measurement therefore seems crucial to recover a clean microelectrode as to continue imaging the sample under study. To overcome this limitation, the SG-TC operation in SECM must be sequentially combined with anodic dissolution steps performed dynamically during scan acquisition, rather than at the end of the scan. But agaom they must be carried out by retrieving the tip from the sample to prevent the released copper ions from reacting with the surface studied. Such potentiodynamic procedures have been performed, although they primarily involved mercury-modified electrodes for battery research [14,15,33], the characterization of soil/solution interphases [20] and model samples releasing heavy metals [34]. The latter was performed by fast scan cyclic voltammetry combined with SECM (FSCV-SECM) capable of almost simultaneously revealing various species (e.g., dissolved oxygen) and surface properties (i.e., feedback mode). The proof of principle of FSCV-SECM has been demonstrated, and the technique has been exploited with bare Pt, Au and carbon fibre microdisc electrodes to assess the biological activity of individual cells (macrophages) [35–37]. But, to our knowledge, no attempt has been made to use a similar potentiodynamic method on material substrates with conventional mercury-free microdisc electrodes.

In the present work, CV-SECM and SWV-SECM were explored as promising methodologies to locally determine the release of Cu^{2+} from copper surfaces subjected to corrosive attack in acidic NaCl solution, avoiding the fouling of the tip resulting from copper conversion on the microdisc. Since a freely corroding surface evolves faster than the time required to record a complete voltammogram at each scan point followed by tip retrieval from the surface for metal stripping, making the process of acquiring each pixel in the scan grid quite long compared to the time scale of surface modification resulting from the corrosion process, the CV-SECM and SWV-SECM methods had to be modified to perform the entire sequence of steps simultaneously to scanning the surface under a constant tip-sample distance condition. Then, in order to avoid local modification of the corroding surface by the stripped copper ions in the confined electrolyte volume between the tip and the sample, the tip must move parallel to the surface at a sufficiently high scan rate to facilitate mixing by convection. This has been achieved by dynamically coupling the rates corresponding to the movement of the tip during scanning and those of the voltammetric potential sweep. Accordingly, CV-SECM was used to correlate the anodic dissolution of copper with the loss of surface reactivity to charge transfer, taking advantage of SG-TC and feedback responses in selected potential ranges. Next, SWV-SECM was applied to determine copper(II) cations that evolve from pristine copper and benzotriazole-copper model system upon exposure to acidic chloride-containing media.

2. Experimental

A copper foil of thickness 1 mm and 99.99 % purity supplied by Goodfellow (Cambridge, UK) was cut into quadratic prisms and placed vertically in a hollow cylindrical rubber container closed by a wax film at one side, to serve as a mould for embedding the metal in epoxy resin (EpofixKit, Struers, Denmark). The mould was removed after 24 h, offering in the upper part a flat copper surface surrounded by epoxy resin with an approximate area of 1–2 mm^2, while an electrical contact was established with the other end of the copper prism that protrudes from the back of the epoxy sleeve. The surface of the copper sample was mechanically abraded with 800, 2500 and 4000 grit silicon carbide papers, then polished with alumina and rinsed with ethanol in an ultrasonic bath for 10 min and dried in air.

Benzotriazole (BTAH; Avocado Research Chemical Ltd, Heysham, UK) and ferrocenemethanol (Aldrich, St. Louis, MO, USA) were used as received. Analytical grade potassium chloride (KCl), sodium chloride (NaCl), copper chloride ($CuCl_2$), hydrochloric acid (HCl) and sodium perchlorate ($NaClO_4$) were employed to prepare the base aqueous electrolytes. All aqueous solutions were prepared with ultra-pure water purified using a Milli-Q system from Millipore (Burlington, MA, USA). All measurements were performed at room temperature in naturally aerated solutions.

Gold microelectrodes with 10 μm diameter disc embedded in glass capillaries were used for measurements in bulk solution and SECM operation. Conventional electrochemical measurements were performed in the three-electrode configuration, with the gold microelectrode as the working electrode 1 (WE#1), an Ag/AgCl/KCl (sat.) electrode as reference, and a platinum grid as the auxiliary electrode. All potential values in this work are referred to the Ag/AgCl/KCl (sat.) reference. CV and SWV were first performed in bulk solutions in order to evaluate the behaviour of the gold microelectrode, using a μStat 8000 potentiostat (Dropsens, Oviedo, Spain). The parameters for the SWV were: 4 mV step increment, 25 mV pulse amplitude and 20 Hz frequency. The collection efficiency of the Au probe for copper reduction was investigated by adding x mM $CuCl_2$ (with values of x: 0.01, 0.1, 1, 10, and 100) to the 3.5 wt.% NaCl test solution. All tests and corrosion experiments were conducted ensuring that pH was adjusted at 3.5 by adding minute amounts of a concentrated HCl solution.

SECM measurements were performed with a high resolution SECM device (Sensolytics, Bochum, Germany), receiving the analogic outputs of a CHI900 potentiostat (CH-Instruments, Austin, TX) as electrochemical interface, all controlled by personal computer. The electrochemical interface effectively functioned as a bipotentiostat, allowing both the gold microelectrode and the copper sample to be individually biased as WE#1 and WE#2, respectively. The small electrochemical cell was built by fixing with fast-curing silicone a hollow cylindrical methacrylate mould on top of the epoxy resin sleeve that surrounds the copper surface, thus producing a container for approximately 4 mL of the test electrolyte. The electrochemical configuration was completed with an Ag/AgCl/KCl (sat.) electrode as reference and a platinum wire as auxiliary. Ferrocenemethanol was used as the redox mediator for sample localization, establishing the tip height and to image the surface in situ. The electrolyte was 0.1 M $NaClO_4$ + 0.5 mM ferrocenemethanol solution, and the potential of the tip was set at +0.50 V for the diffusion-limited oxidation of ferrocenemethanol. The choice of a chloride-free

solution for this *ex situ* step aimed to avoid the initiation of copper corrosion during this positioning step. First, the operating tip-substrate distance was established using the feedback mode of SECM by recording several approach curves at selected locations on the sample above the surrounding epoxy resin sleeve, ensuring that tilt was negligible. In this way, precise sample positioning and tip-sample distancing were achieved.

Once the tip was retrieved to a safe and controlled distance from the substrate, electrolyte replacement was conducted by replacing the solution with 3.5 wt.% NaCl (pH 3.5) as the test environment. Inhibition tests and feedback mode response were investigated by adding 1 mM BTAH and 0.5 mM ferrocenemethanol to this solution, respectively. During this step, the SECM was operated using the bipotentiostat option, so that the substrate potential could be controlled at desired fixed values as WE#2, whereas potentiodynamic perturbation was continuously applied to the rastering SECM probe at 30 μm s^{-1}. That is, the probe was moving in the *X-Y* plane while simultaneously conducting voltammetric measurements. This potentiodynamic perturbation at the tip consisted of either cyclic voltammograms (CV−SECM) between −0.50 to +0.50 V vs. Ag/AgCl/KCl (sat.) at a sweep rate of 0.1 V s^{-1}; or square wave voltammograms (SWV−SECM) from −0.40 V to +0.50 V vs. Ag/AgCl/KCl (sat.) using the same parameters as described above for the tests in the bulk solution. While scanning in the SWV-SECM mode, unless otherwise stated, each SWV was preceded by a 10-second deposition step at −0.40 V vs. Ag/AgCl/KCl (sat.). This manner, the SG-TC mode was exploited to collect the releasing Cu^{2+} ions upon intermittent application of cathodic potential, and next the metallic copper was anodically redissolved from the probe during the same scan acquisition.

3. Results and discussion

3.1. Electrochemical behaviours of gold electrodes for copper collection

The UPD response of gold macroelectrodes toward copper(II) is well characterized, and the shape of the CV has also been explained in the case of gold microwires [38–41], while gold microdiscs have been mainly employed with pulsed stripping techniques [26,42]. Yet, it should be noted that, if the gold microelectrode was to be employed as the measuring tip for SECM operation, the tip will be placed in close proximity to the surface being studied, thus confining a very small volume of electrolyte solution between the tip and the sample. Next, corrosion processes result from the establishment of local microcells of micrometric (and sometimes even submicrometric) dimensions [43]. Since the anodic sites are initially limited in extension and activity, the dissolved metal ion concentrations can be found smaller than ppm in the bulk of the electrolyte [44]. However, all of these ions arise from a very small surface area which, when placed under the tip of the SECM, defines a minute volume of electrolyte. Consequently, it is in this highly concentrated electrolyte that potentiometric measurements have shown concentrations sometimes of the order of 1 mole per litre [25,45,46]. As the objective of this work is to identify and monitor reactive sites, a possible accumulation of high local concentrations below the tip must be expected. Therefore, a concentration of Cu^{2+} ions of 100 mM was considered feasible and adequate for the characterization of the electrochemical behaviour of a gold microelectrode for tip operation in SECM. A 10 μm diameter gold microdisc electrode was then evaluated in 3.5 wt.% NaCl solution as well as with the addition of 100 mM $CuCl_2$, and it is shown in Fig. 1. The labels indicate the sequence of events during the measurements, started from 0 V (labelled as *1* in the Figure) and first reversed at −0.50 V.

In the absence of dissolved copper, only the onset of the O_2 reduction wave was observed in the selected potential window (red curve and inset in Fig. 1), as expected. For the voltammogram measured in the solution containing 100 mM $CuCl_2$ (black curve), the onset of copper reduction is seen from potential corresponding to label *2*, reaching an inflection point that reflects mass transfer (diffusion) control at ca. −0.30 V (label

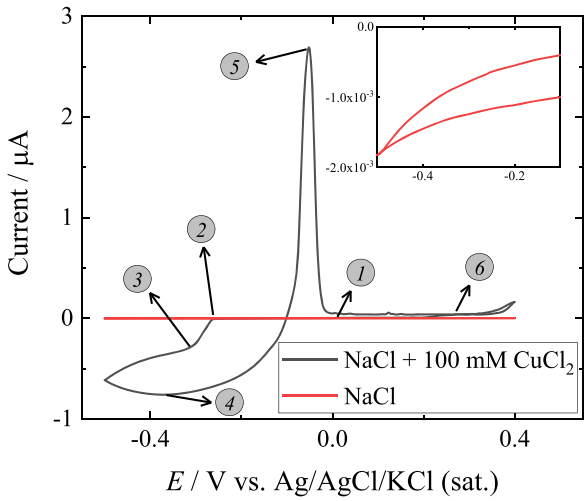

Fig. 1. Cyclic voltammograms (CV) recorded for a gold microelectrode in 3.5 wt.% NaCl and in 3.5 wt.% NaCl + 100 mM $CuCl_2$ solutions (acidified to pH 3.5). The inset shows an amplification of the plot obtained in the 3.5 wt.% NaCl solution (i.e., without $CuCl_2$.). Potential sweep rate: 0.05 V s^{-1}. Diameter of the gold microdisc electrode: 10 μm. See the body of the manuscript for the meaning of labels *1–6*.

3). From this point, the Cu^{2+} ions that reach the microelectrode are electrodeposited on its surface, thus increasing its active area and subsequently the detected cathodic current. This increase in cathodic current is observed even after reversal of the potential sweep, before a reoxidation peak occurs when potential is sufficiently anodic. Such observation of increasing cathodic current despite reversal of the potential ramp before anodic stripping is consistent with other reports on the deposition and dissolution of copper on gold microelectrodes in aqueous or ethanolic solutions [30,47], also common for platinum sensors [48,49].

The continuous electrodeposition of copper that occurs between labels *2* and *4* limits the validation of the concentration estimations from current responses, as constrains apply since the microdisc dimensions do not remain constant. Such estimations could only be considered feasible for the limiting current measured just at the inflection point at label *3* (at approximately –0.30 V in Fig. 1), when the copper has not yet modified the surface morphology of the gold microdisc. Here, the current is expected to follow the equation:

$$i_{lim} = 4nFDcr \quad (1)$$

where i_{lim} is the limiting diffusion-controlled current, F is the Faraday constant, n the number of exchanged electrons, D the diffusion coefficient of the converted species, c its concentration, and r the microdisc radius. Although monovalent copper species are expected in chloride-rich environments, it can be assumed that cathodic potentials of –0.30 V or greater lead to the exchange of two electrons [50–52]. Therefore, considering a diffusion coefficient value of 6.20 × 10^{-6} cm^2 s^{-1} for Cu^{2+} in aqueous solution [53], the current recorded at –0.30 V in Fig. 1, which amounts −0.25 μA, gives an apparent concentration value of 105 mM, in good agreement with the concentration of copper available for reduction in the solution.

Concerning the response in the SWV, Fig. 2 illustrates the optimization of the deposition time (t_d) at −0.40 V for a solution containing 0.1 mM $CuCl_2$. The oxidation peaks are observed in two different potential ranges, namely $-0.20 < E < 0$ V and $0.30 < E < 0.40$ V. According to the literature, the peaks appearing for $0.30 < E < 0.40$ V correspond to the oxidation of the copper collected by underpotential deposition (UPD), a signal frequently exploited for copper quantification using gold electrodes [53–55], including microwires [26,38,41,56] and microdisc geometries [29]. Indeed, all of these studies demonstrate the

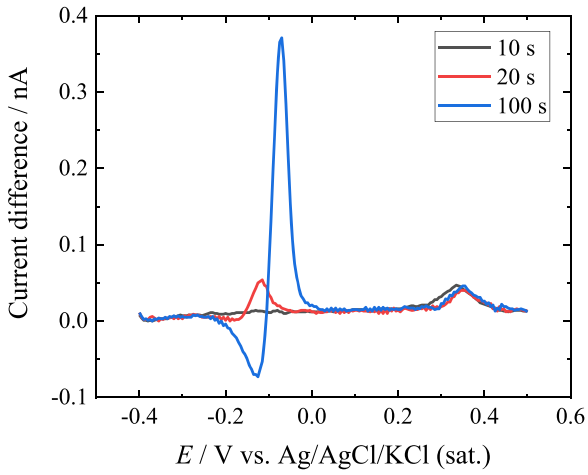

Fig. 2. Square wave voltammograms (SWV's) recorded for a gold microelectrode in 3.5 wt.% NaCl + 0.1 mM $CuCl_2$ solution (acidified to pH 3.5) for different deposition times as shown.

possibilities for copper determination down to the micromolar range, rather than the higher millimolar concentration values considered in this work, which can otherwise be found locally at actively corroding surface sites as described before [25]. In contrast, voltammetric peak signals in the potential window $-0.20 < E < 0$ V are less frequently reported in the literature [57]. In our observations, the deposition time appears to only affect the signals recorded at less positive potentials, while the size and shape of the peak in the expected range around +0.35 V remains unchanged. Assuming that the latter actually corresponds to the signal resulting from the reoxidation of the copper collected by UPD, that is to say the first monolayer of copper deposited directly on the surface of the gold microdisc, it is reasonable that the surface of bare gold becomes saturated with copper after a rather short deposition time. In contrast, signals with lower anodic potentials ($-0.20 < E < 0$ V) may arise from oxidation in which Cu-Cu bonds are broken under less energetic conditions. This is supported by previous observations in the literature using microdisc electrodes [42,58], where the matrix effect was suggested to be the responsible phenomenon. In fact, variations in concentration and deposition time ranges revealed features aligned with the possible duplicity of peaks when the gold surface reaches apparent saturation [59], which was proposed as the most likely result when using AFM-SECM electrodes for the calibration of copper concentration based on the potential deposition signal [31,32]. With those very small electrode areas, the signals arising from the UPD may thus become negligible compared to the signal resulting from the cleavage of Cu-Cu bonds.

In fact, simple application of Faraday's laws and use of common physicochemical properties of copper (i.e. atomic weight 63.546 g $mole^{-1}$, density 8.96 g cm^{-3}) predict that a total charge of 6×10^{-10} C is enough to theoretically achieve the formation of a compact copper monolayer with a thickness approximately equal to the diameter of one copper atom (i.e., 280 pm). In theory, no more than 2.5 s deposition time is required if a limiting current of –0.24 nA is maintained, which results from applying Eq. (1) for the conversion of 0.1 mM Cu^{2+} at the probe. For the geometric conditions of the gold microdisc, the selected potential of –0.40 V may be sufficient to achieve approximate diffusion-controlled current values (see Fig. 1). Thus, only the stripping peaks recorded below –0.10 V in the voltammogram of Fig. 2 and other results of this work, resulting from the breakdown of Cu-Cu bonds, would provide information which is not limited by the saturation coverage of the gold microdisc surface (i.e. it is not from copper UPD). Then, to avoid excessive copper deposition, which would severely modify the morphology of the probe during scanning, a deposition time of 10 s was selected for the SWV-SECM operation.

Although quantitative calibration is beyond the scope of this work, the trends of the signals with respect to the Cu^{2+} concentration in the bulk solution were tentatively explored using the scarce data available in the literature. By using semi-logarithmic plots, the integrated peak areas (determined from CV and SWV measurements) and the limiting current reached at ca. –0.30 V (from CV measurements) were correlated to the concentration of copper ions in Fig. 3. Dotted lines reflect linear fits for all the parameters ($R^2 = 0.999$), except for the integration of the SWV peak in the potential window corresponding to the oxidation of the Cu-Au bond (labelled Q_1 in Fig. 3B, left axis). The latter is affected by the saturation of the gold microdisc. The slope of the proportional trend between i_{lim} and concentration (Fig. 3A, right axis) gives 2.49 nA mM^{-1}, close to the theoretical value of $4\,n\,F\,D\,r = 2.39$ nA mM^{-1} according to Eq. (1). Although these results should be taken with caution due to lack of analytical merits and validation, they demonstrate the ability of the technique to provide at least semi-quantitative information on the copper content from rapidly evolving Cu^{2+} sources. Care must be taken as complete recovery of the gold microdisc cannot be guaranteed, while the formation of copper oxides and/or detachment of copper clusters must be examined in more detail to address multiscale quantification. Additional information on the linear fits derived from the semi-quantitative estimations presented here is included in the Section S.1 of the Supporting Information, demonstrating the promising effectiveness of the methodology proposed here.

3.2. CV-SECM study of copper corrosion in chloride solution

The information accessible via the variety of SECM modes depends on the system under study and the electrical conditions attained by the probe and the substrate. Therefore, multiple parameters can be accessed sequentially by selecting potentiodynamic methods, i.e. performing CVs at the probe sensor while rasterizing the surface of the substrate in a coupled methodology as proposed in this work, that is actually a modification of the known CV-SECM operation. The following novelties were envisaged: (1) the tip-substrate distance is always kept constant throughout the measurement process, including the deposition and redissolution steps that occur at the tip during the voltammetric operation in each cycle. And (2) the SECM tip continuously scans the surface, while the potential of the tip is scanned at a different sweeping rate for the voltammetric operation. In this way, the deposition stage occurring at the tip (corresponding to the active dissolution from the corroding surface below), occurs at different locations of the surface studied from those where the tip is during the redissolution stage (and no information is obtained from the surface location just below). This methodology involves some loss of spatial resolution because not all the points in the *X-Y* grid will be rasterized while the tip is actually in the collecting region of the voltammograms. Then it is necessary to combine the spatial rasterization rate with the sweep rate of the voltammetric measurement, so that the points along one line of the grid without information on the corrosive process (corresponding with the stripping stage at the tip), can become accessible in the following line, when the tip passes near those location while in the collection potential range of the sweep. Although this is a simplified description, because there are other potentials values in the voltammetric range where the tip neither collects nor redissolves copper, this can be taken as an advantage for the method proposed in our work. Fig. 4 shows sketches of the measurement principle applied for a zig-zag (so-called, *meander*) movement of the SECM tip, as applied in a real measurement within this work. This scheme also takes into account the time required for the software to acquire the current and potential data point for each grid position; the scanning rate of 30 μm s^{-1} applies when tip moves from one point to the next.

Although this method effectively reduces the spatial resolution in the *X-Y* scan map, since only collection of dissolving metal will occur at certain places during each line (and not actively collecting data at all the points along the line), it should allow a sufficiently fast collection of data to properly identify and monitor the position of the active front or sites

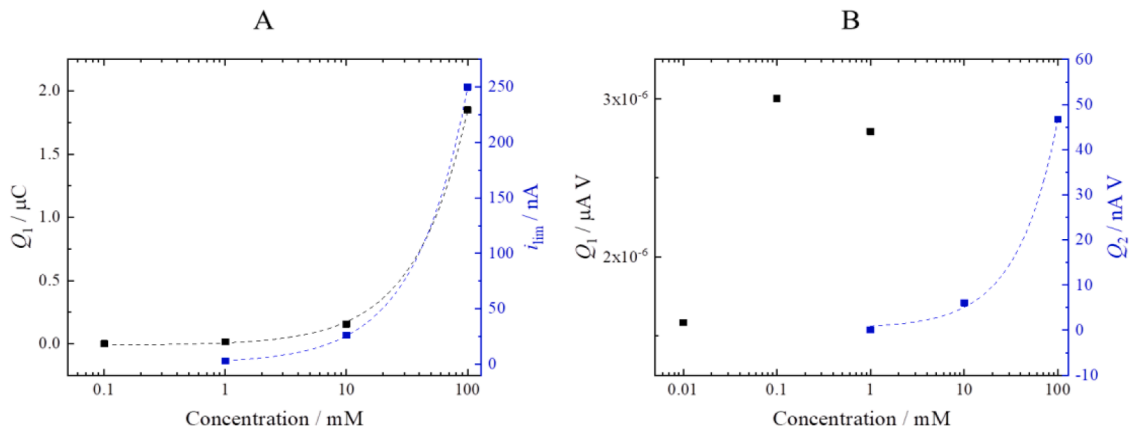

Fig. 3. Quantitative information extracted from (A) CVs and (B) SWVs recorded with a gold microelectrode in the bulk of 3.5 wt.% NaCl solutions (pH 3.5) with different concentrations of $CuCl_2$ [57]. (A) Results of the integration of the peak at approximately –0.10 V (Q_1, left axis) and the limiting cathodic current (i_{lim}, right axis) at –0.30 V. (B) Results of the integration of the peak signals recorded in the potential windows $0.30 < E < 0.40$ V (Q_1, left axis) and $-0.20 < E < 0$ V (Q_2, right axis).

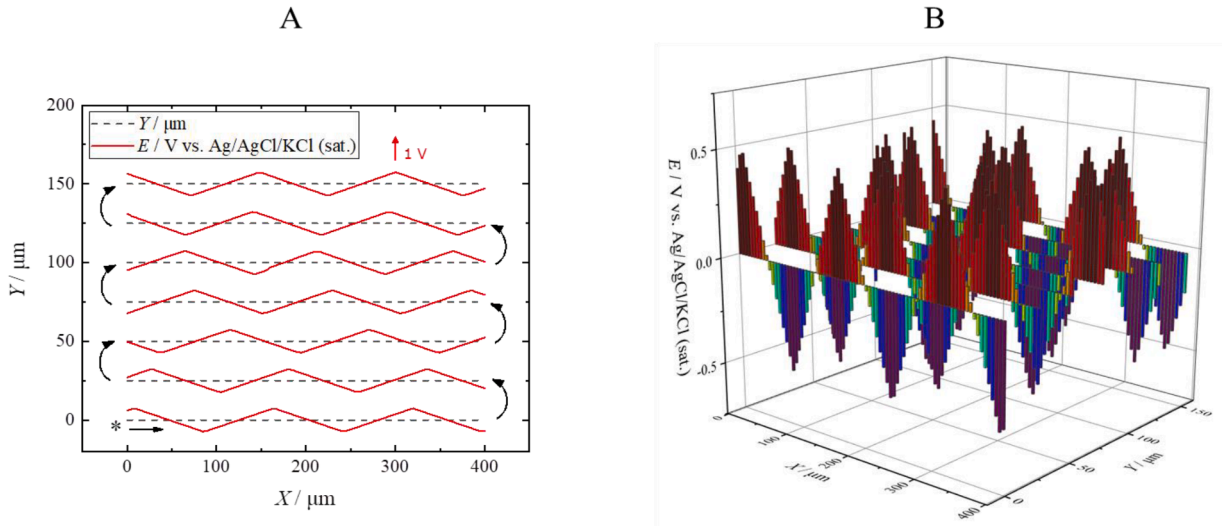

Fig. 4. Schematics of the potentiodynamic method based on CV-SECM proposed in this work. (A) 2D schematics with starting position labelled as *, dashed lines and black arrows indicate the tip position and movement in the *zig zag* (so-called, *meander*) mode. (B) 3D schematics reflecting the actual potential at each *X-Y* position. Voltammetric scans are not collected at each point of the *X-Y* scanning grid, but they are continuously recorded in a coupled way to the motion of the tip. Scan rate: 30 µm s^{-1} in the *X* direction. Potential and current data-points are collected by the Sensolytics Software every 5 µm.

in a dissolution process.

For CV-SECM operation, a primary consideration is the need for sufficient copper release for detection by the occurrence of a reoxidation peak such as those observed in Fig. 2. The associated features were investigated using a copper surface shown in Fig. 5A, scanning the 500 × 500 μm^2 area inside the yellow square drawn on this figure. Fig. 5B shows the initial feedback scan recorded under potentiostatic conditions (with the probe sensor polarized at +0.50 V) and maintaining the substrate in its OCP in a solution of $NaClO_4$ that contains ferrocenemethanol, that is used only for surface location. The solution was then carefully replaced with the test solution (acidified 3.5 wt.% NaCl, pH 3.5) also containing ferrocenemethanol as a redox mediator. A series of CV-SECM scans were recorded while rastering the SECM probe above the sample. Meanwhile, the copper substrate was held at a constant potential. Figs. 5C and 5D show typical CV measurements acquired by scanning over the insulating resin, the boundary region, or the copper surface while polarized at −0.15 or −0.10 V, respectively. It is clear that the increase of the anodic overpotential for WE#2 from Fig. 5C to 5D favours the release of Cu^{2+}, generating a diffusion-limited cathodic signal accompanied by a reoxidation peak as the probe passes over the copper surface.

Conscientious data processing and evaluation allowed the different electrochemical signals of the CVs to be assigned to corresponding tip positions on the scanned area. Although the intercomparison of such signals is not straightforward, their representation relative to the probe location allows a local estimation of the extent of copper degradation. A small cathodic peak was observed at the tip potential of −0.20 V in Fig. 5C under mildly corrosive conditions, and the diffusion-controlled current around −0.35 V observed in Fig. 5D for strongly anodic substrate polarization. Both of these signals could be attributed to concentration gradients of local release of Cu^{2+} ions, although the cathodic signal in Fig. 5C must be taken with caution as the response is likely to be affected by the onset of oxygen reduction, and in particular by progressive modification of the microdisc morphology while scanning. Fig. 6 shows the values of the electrochemical signals observed in Figs. 5C and 5D monitored during scan acquisition, limited to an area of interest of 400 × 400 μm^2 to optimize scan duration. The signals shown are associated with the local release of copper cations via (*i*) the cathodic peak area in Fig. 6A, of the peak around −0.20 V in Fig. 5C; (*ii*) the diffusion cathodic current in Fig. 6B, of the cathodic current around

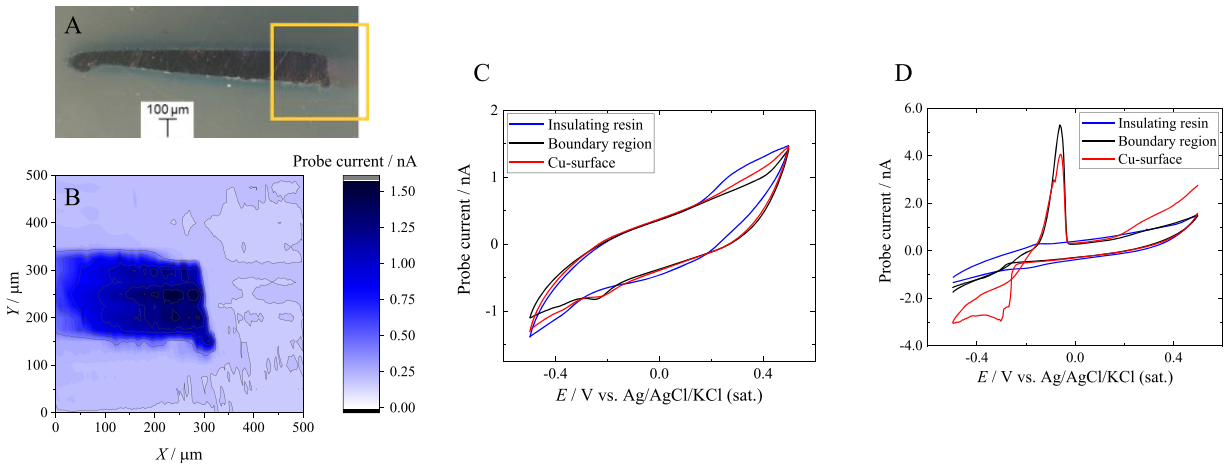

Fig. 5. (A) Optical image of the studied copper surface. (B) SECM map in feedback mode of the yellow square drawn in (A) while the sample was exposed to a solution of 0.1 M $NaClO_4$ + 0.5 mM ferrocenemethanol. (C, D) CV measurements obtained at the SECM probe when scanning the sample in the vicinity of the insulating region, the boundary region or on metallic copper, as indicated in the legend, all immersed in acidified 3.5 wt.% NaCl solution (pH 3.5) containing 0.5 mM ferrocenemethanol. The electrical conditions of the copper substrate were: (B) at its spontaneous OCP, or polarized at (C) −0.15 and (D) −0.10 V. Tip-substrate distance: 10 µm; tip diameter: 10 µm; CV scan rate 0.1 V s^{-1}; SECM scan rate: 30 µm s^{-1}.

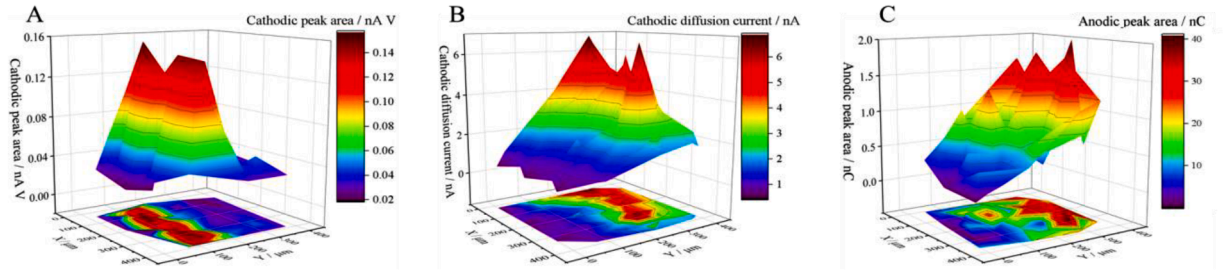

Fig. 6. Electrochemical signals recorded during CV-SECM measurements of the area located in the yellow square in Fig. 5A. (A) Cathodic peak area from the peak around −0.20 V in Fig. 5C. (B) Diffusion cathodic current from the cathodic peak around −0.35 V in Fig. 5D. (C) Anodic peak area from the anodic reoxidation current in Fig. 5D. Copper substrate exposed to acidified 3.5 wt.% NaCl solution (pH 3.5) containing 0.5 mM ferrocenemethanol, and polarized to: (A) −0.15, and (B, C) −0.10 V. Tip-substrate distance: 10 µm; tip diameter: 10 µm; CV scan rate: 0.1 V s^{-1}; SECM scan rate: 30 µm s^{-1}.

−0.35 V in Fig. 5D; and (*iii*) the anodic peak area in Fig. 6C, of the anodic reoxidation current seen in Fig. 5D.

The measurements shown in Fig. 6 demonstrate that copper(II) is mainly collected around a central region of the scanning area, where the copper surface is actually placed. Disturbances due to diffusion and convection caused by the tip movement appear to cause distortion in a more precise location of the active zone. Furthermore, the peaks seen in all three figures indicate more intense Cu^{2+} dissolution at localized sites, likely corroding pits, particularly for the copper electro-reduction signal in Fig. 6B with copper polarized at −0.10 V. The signal in Fig. 6C has lower resolution, mainly due to the difficulty in assigning a probe location for the reoxidation of the copper collected during the previous cathodic scan. Despite this limitation, the image obtained agrees with the expectations, and considering that the main objective of the reoxidation step is to recover a clean surface of the microelectrode rather than to locally quantify the copper content, these measurements could be considered satisfactory for a semi-quantitative chemical and spatial determination of the extent of degradation. A local estimation can be further attempted by considering the signals and prior characterization of the probe response in the bulk solution (Fig. 3A), based on the parametric data provided in the Supporting Information (Section S.1). The limiting currents of 3 to 7 nA found in Fig. 6B then correspond to concentrations of 1.2 to 3 mM, respectively, while the local signals of 10 to 40 nC in Fig. 6C correspond to concentrations of 2.1 to 5 mM.

The signal from the probe potentials that normally correspond to ferrocenemethanol oxidation (that is, corresponding to a feedback response) could also be extracted from the continuous CV measurements in Figs. 5C and 5D, taking advantage of the intended presence of this mediator in the solution. The current of the probe when its potential reached the maximum value of +0.50 V varied from scan to scan depending on the kinetic constant for the electron exchange [12,60]), its conductivity (hindered by the formation of passive layers) and the controlled electrical state of the substrate. This is visible in Fig. 7 by the feedback current detected at the tip when scanning the substrate with the copper polarized at increasing potentials from −0.20 (Fig. 7A) to −0.10 V (Fig. 7C).

The feedback effect observed when copper was polarized at −0.15 V, shown in Fig. 7B, was poorly resolved, mainly due to greater heterogeneity in the surface distribution of the kinetic ability for electron transfer. However, a significantly higher signal was recorded in the central part of the scanned area, revealing higher conductivity. In the case of the sample subjected to the most anodic polarization (Fig. 7C), the feedback effect was very localized and represented current values up to 10 nA. Again, diffusion and convection effects can make precise signal localization difficult, which is further hampered by the heterogeneous nature of the copper surface as it degrades. This characteristic reflects that, although the electrical state of the sample favours a lower tendency to donate electrons due to the lower cathodic potential applied substrate, this is compensated by the formation of a less compact passive layer, which has greater conductivity leading to facilitated charge transfer at the active sites. The continued release of copper(II) under these conditions, according to the concentration distribution responsible

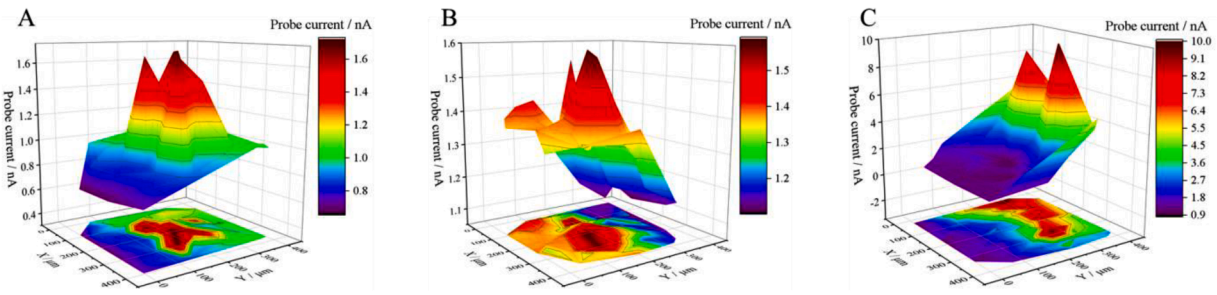

Fig. 7. Probe current signals recorded during CV-SECM measurement scans of the area in the yellow square in Fig. 5A when the potential of the SECM probe reached +0.50 V. Copper sample exposed to acidified 3.5 wt.% NaCl solution (pH 3.5) containing 0.5 mM ferrocenemethanol, and polarized to: (A) −0.20, (B) −0.15, and (C) −0.10 V. Tip-substrate distance: 10 µm; tip diameter: 10 µm; CV scan rate 0.1 V s^{-1}; SECM scan rate: 30 µm s^{-1}.

for the results in Figs. 6B and 6C, correlates well with the decrease in the protective character of the passive layers, thus facilitating electron exchange. In contrast, the lack of a distinct Cu^{2+} distribution at the substrate potential of −0.20 V (not shown) was accompanied by a more conductive substrate that was still kinetically capable of promoting reoxidation of ferrocenium ions on the copper surface (see Fig. 7A). However, an anodic dissolution of Cu^{2+} ions from the polarized substrate was to be expected, since −0.20 V means sufficient anodic overpotential for copper to locally release copper(II) cations [32], although the CV-SECM method used may not be sensitive enough to detect small amounts of this chemical species.

3.3. SWV-SECM study of copper corrosion and inhibition in chloride solution

In order to improve the sensitivity of the potentiodynamic technique towards copper(II) cations under less aggressive conditions, the SWV-SECM mode was adopted although it was insensitive to the feedback effect that could be employed with CV-SECM. Similar to our method for CV-SECM, achieved by continuous sweeping of the potential and at the same time maintaining the raster of the tip, in our case SWV-SECM performs deposition and anodic stripping without stopping the movement of the tip. SWV was not recorded at every point of the grid, but each deposition-stripping application took less than completing one line in the grid. This method was implemented using a copper sample initially imaged in a similar manner to that employed in Fig. 5B. The cell was then washed and the electrolyte solution was replaced with the corrosive acidified 3.5 wt.% NaCl solution (pH 3.5) without losing the probe position, and a 500 × 500 $µm^2$ potentiodynamic map was recorded. No redox mediator was added to this solution because the SWV measurements were not expected to clearly provide a feedback response. Throughout this measurement, again distributed over a region of the same or equivalent geometry, a series of SWV runs were recorded continuously until the collection of the SECM map was completed.

In a first data visualization approach, similarly to the graphs shown in Fig. 5C and 5D, the SWVs were extracted from areas where the probe moved mainly over a region in the absence of copper (named as zone I), when the probe approaches the boundary between the resin and the surface of copper (zone II), and when the tip is mostly on the metal (zone III). The information related to each of them will be extracted from the

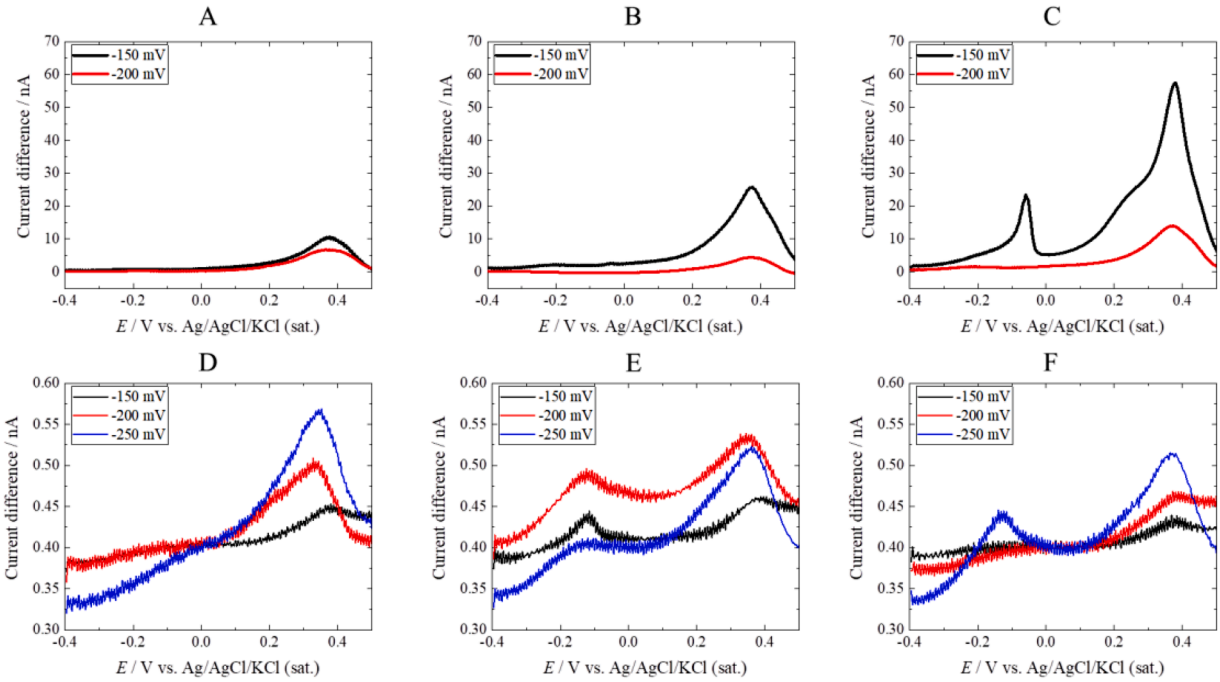

Fig. 8. SWVs recorded with a gold microelectrode moving over a copper sample exposed to 3.5 wt.% NaCl (A, B, C) in the absence and (D, E, F) in the presence of 0.5 mM BTAH. The copper substrate was polarized as indicated in the legends. The SWVs were recorded while the tip travelled over the scanning zones corresponding to: (A, D) the insulating resin, (B, E) the boundary region between resin and copper surface, and (C, F) the copper surface. Tip-substrate distance: 10 µm; tip diameter: 10 µm; SECM scan rate: 30 µm s^{-1}.

SWV measured in the absence and in the presence of BTAH, at different polarization potentials applied to the substrate (see Figure S2 in the Supporting Information). The voltammograms in Fig. 8 correspond to measurements made in the 3.5 wt.% NaCl solution, either in the absence (A to C) or in the presence (D to F) of 0.5 mM BTAH. It should be noted that the graphical scales vary by two orders of magnitude for the current between the two experimental series, since the maximum difference in tip current measured in these voltammograms was 57 nA and 0.57 nA in the solutions without and with inhibitor, respectively. This reflects the proven effectiveness of BTAH as a corrosion inhibitor for copper.

Interestingly, the signals in the absence of BTAH reveal reoxidation peaks in the potential range $0.30 < E < 0.40$ V, much larger than those registered as maxima for the complete coverage by copper of the gold surface that was deposited in the bulk solution in Fig. 2. This fact apparently contradicts the gold saturation hypothesis, preventing the analysis of the peak after UPD. The reasons behind this phenomenon require further investigation, although they are likely related to the presence of the inhibitor and the subsequent presence of additional species resulting from corrosion of the copper surface, such as Cu(I)BTA or CuCl adsorbates, which could be next electrochemically converted at the probe [61]. The probe is expected to slightly shift the onset potentials for deposition and reoxidation, and it is unlikely to be recovered as a pristine gold surface. Therefore, only a qualitative discussion can be considered at this stage and additional experiments are needed to provide sufficient information for a quantitative estimation.

From a cursory observation of Fig. 8A to 8C, that is to say in the absence of corrosion inhibitor, we can see that the more negative is the potential applied to the substrate, the smaller is the observed release of copper(II) ions from the sample in all the three zones. Furthermore, as expected, the larger the area of metallic substrate covered during the SWV acquisition in each section (mainly in sector III, cf. Fig. 8C), the greater the quantity of reoxidized copper detected at the tip. When the solution contains BTAH (see Figs. 8D to 8F), the same trend of increasing current is observed with increasing presence of copper surface for each sector, but the opposite trend is observed with respect to polarization of the substrate. That is, the measured current coming directly from copper dissolution is higher when more negative potentials are applied to WE#2 (which would result in greater cathodic protection in the absence of the corrosion inhibitor). This is explained by the mechanism of formation of the inhibitor film, which would depend on the aggressiveness of the applied conditions, such as chloride anions and applied potential, according to reports [10,62]. The formation of the protective polymeric layer containing the inhibitor is further promoted by the increased release of copper ions as the key for the formation of the Cu(I)BTAH complex as a rate-limiting step. The interaction of the inhibitor, particularly with the electrodeposited copper during its detection, may also play a role [61]. As an additional observation, even when the quantities of copper detected were very low, we can observe the appearance of signals in the potential range corresponding to the breakdown of Cu-Cu bonds (cf. Figs. 8D-E). This indicates that the deposition of copper on the gold microdisc did not occur uniformly; in other words, the reduction of Cu^{2+} can take place from small regions of the microelectrode in which the copper has previously been deposited, without it being necessary to cover the entire gold surface.

The conditions of the SWV-SECM measurements, in terms of deposition time, tip movement speed and duration of the potential scan, were optimized and analysed so that each reoxidation signal could be correlated to tip positions on the scanned area, which allowed the acquisition

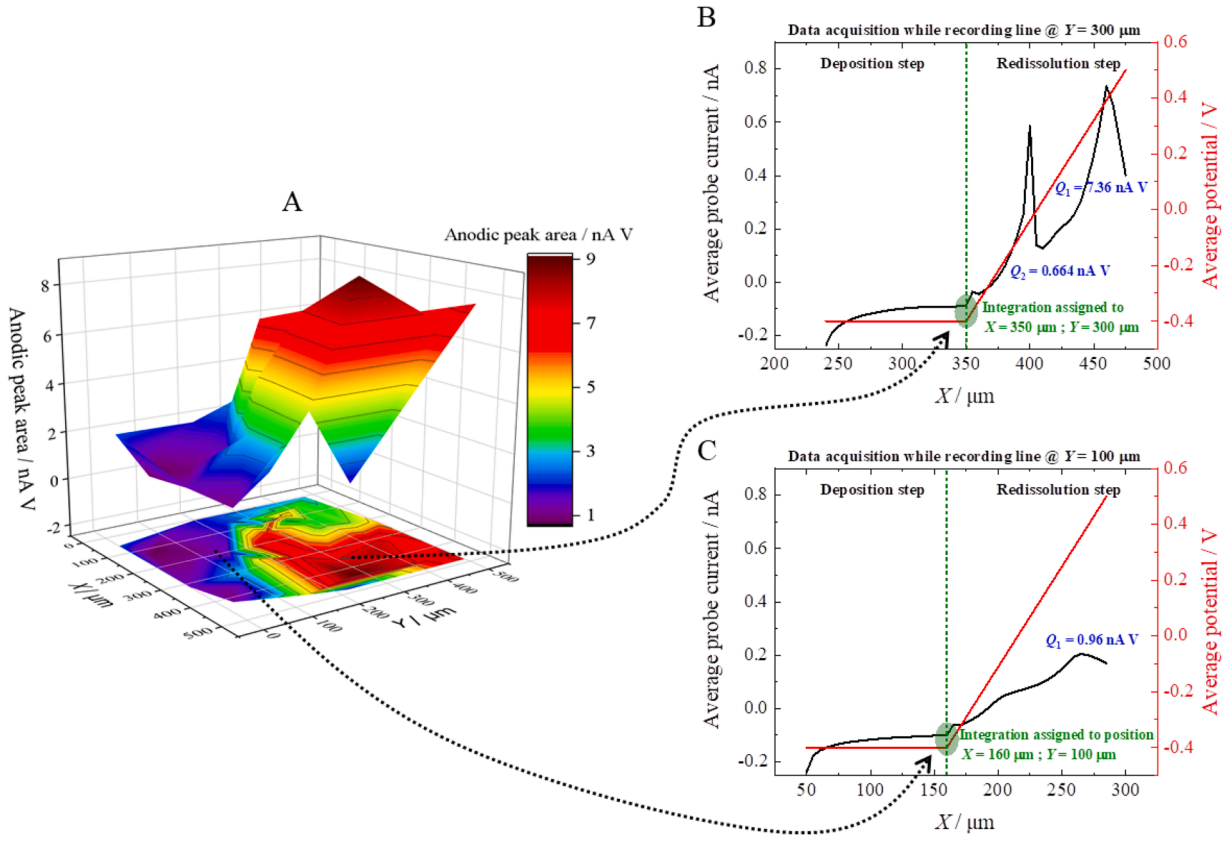

Fig. 9. (A) SWV-SECM map of a copper sample immersed in acidified 3.5 wt.% NaCl (pH 3.5). The colour scale reflects the values of the peak areas scanned with the tip polarized at +0.35 V. (B,C) Graph of the average probe current (black line, left axis) and average probe potential (red line, right axis) when scanning in the *X* direction at positions: (B) $Y = 300$ µm and (C) $Y = 100$ µm in the map of Fig. 9A. Each graph shows the values of the corresponding peak areas in the SWV measurements as well as the *X* position where the peak value was assigned. Scanned area: 500 × 500 µm^2. Polarization of the copper sample: −0.15 V. Tip-substrate distance: 10 µm; tip diameter: 10 µm; SECM scan rate: 30 µm s^{-1}.

of a chemical image of the released copper cations. Fig. 9A shows the scan image obtained by integrating the tip current values recorded over a copper surface polarized at −0.15 V during its immersion in the acidified NaCl solution without corrosion inhibitor. For map visualization, the reoxidation peak corresponding to a tip potential of +0.35 V was considered. The peak area expressed in A V was plotted as a function of the tip position (*X,Y*) at the end of an optimized 30-second deposition step at −0.40 V. After each deposition step, the tip experienced anodic stripping using SWV. During this anodic dissolution step, no net reduction or oxidation of copper occurs between approximately –0.40 and ca. –0.20 V and the reoxidation steps initiated subsequently give the integrated peaks and ensure copper redissolution. Since the Cu^{2+} ions generated from the substrate are collected while the deposition steps occur at the tip, the actual integration of the copper peak must be ascribed to the locations where the tip was actually collecting (compared to other locations where the tip reoxidizes the collected species). To assign a specific point location, we selected the last location were the tip performed that deposition as shown by the green ellipses in Figs. 9B and 9C. For example, Fig. 9B shows one deposition-acquisition sequence in SWV performed along the $Y = 300$ μm line when the tip moved towards the positive direction of the *X* axis. Copper deposition started when the tip was at $X = 240$ μm and ended when the tip reached $X = 350$ μm. The $X = 240$ to 350 μm conveys the deposition step at the tip, and the position where the signal was next ascribed in the map in Fig. 9A is $X = 350$ μm. This is the only position for the data point considered in the map coming from the entire measurement seen in Fig. 9B, but the signal on the vertical *Z* axis of the map originates from the subsequent reoxidation (not from the previous collection) step. Then, stripping commences and no net current signal was observed between $X = 350$ and 380 μm (cf. Fig. 9B), whereas reoxidation (i.e., copper stripping) occurred as the tip travelled from $X = 380$ to 475 μm. For the complete $Y = 300$ μm line, one more measurement was made just before that seen in Fig. 9B, but no more than 2 or 3 points were taken for each line, with some consequent loss of resolution. Despite the loss of resolution compared to what is usually achieved using a tip diameter of 10 μm, the quick scanning of the investigated surface and the monitoring of data showing differences in reactivity across the material are major advantages that were not feasible until now for a corroding material such as copper and its alloys.

This manner, the values of the red lines in Figs. 9B and 9C are read on the right axis representing the average tip potential during the deposition and reoxidation stages; while the black lines correspond to the left axis and reflect the average current signal from the probe during the measurement. Note that these two graphs plot the average current and potential values recorded via the analogue outputs of the CH Instruments electrochemical workstation feeding the inputs of the SECM interface (which correlates the electrochemical signal with the position of the probe). However, the resolution of such analogue data collection was not sufficient to reflect the pulses applied during SWV measurement in Sensolytics software. As for the *X* axis, it represents the actual position of the tip when scanning a single line at the given *Y* position indicated in each graph. Thus, Figs. 9B and 9C reflect this strategy with each potentiodynamic signal recorded during rasterization over the copper surface (see Fig. 9B for the individual SWV recorded for $Y = 300$ μm) and on the resin (cf. Fig. 9C for an individual SWV registered while travelling for $Y = 100$ μm). Accordingly, the scan acquisition in Fig. 9A provides a semi-quantitative image of copper dissolution as the sample is scanned. A similar scan was recorded in the presence of 0.5 mM BTAH, although no significant values could be recorded for the peak areas due to the inhibitory effect of this species (not shown).

The integration of these peaks is also given with the graphs in Figs. 9B and 9C, which depict data in the order of nA V, estimated relative to the apparent baselines defined by the average current response. Reoxidation at approximately –0.10 V, attributed to bulk copper reoxidation, only results in a clear signal above the copper surface, representing 0.664 nA V, corresponding to an approximate copper concentration of 0.4 mM. However, this quantification is not completely reliable due to the distinctive behaviour leading to the appearance of a clearer copper reoxidation signal around +0.35 V, which was not registered for this concentration range in the bulk solution. Overall, the SWV-SECM operation mode exhibits higher sensitivity for the determination of copper dissolution at a slightly anodic potential than the previous CV-SECM approach, although the latter may provide additional simultaneous information from a feedback response. The difference between the voltammograms obtained for the different sections in Fig. 8 shows that the SECM is capable of performing surface analyses on different zones, since it is able to differentiate the signals collected in a study area of 500×500 μm^2. Fig. 9 finally shows that the method can be exploited to further localize the source of metal cations during their anodic dissolution, thus contributing to the goal of continuing to advance the search for methodologies to increase the spatial resolution of highly sensitive measurements for the quantification of corrosion products.

4. Conclusions

SECM has been used as a microelectrochemical technique for the analysis of electrochemically active substrates and their surface properties, combining, for the first time, electrochemical potentiodynamic control of the corroding material with the application of voltammetric methods at the scanning tip. The voltammetric techniques include square wave voltammetry (SWV) and cyclic voltammetry (CV), although coupled in the potential scan with the movement of the tip, advancing the search for new modes to chemically characterize surfaces in corrosion reactions. The proposed experimental methodology was shown to be applicable both when the corroding substrate is at spontaneously corroding OCP, as well as when polarization was applied to the user using the bipotentiostat built in the SECM configuration.

It has been observed that the electrochemical behaviour of the gold microelectrode is modified when its surface becomes completely covered by the deposited copper, especially when considering millimolar concentrations. Overall, quantitative estimates of the copper content in solution from dissolving metal surfaces appear accessible using these potentiodynamic scanning method.

Thanks to the SWV-SECM combination, it was possible to image the effectiveness of BTAH as a corrosion inhibitor for the protection of copper substrates against corrosion in weakly acidic environments and in the presence of chloride anions. The results showed that the more aggressive the conditions imposed to the copper surface, the greater the protection apparently provided to the material. Further inspections of the inhibitor interaction during electrodeposition are necessary to confirm the formation of protective layers.

Analysis of the potentiodynamic SECM results allowed the copper reoxidation current values to be correlated with the locations of the probe, revealing the dissolution of even small amounts of copper from the surface. The limitations of the proposed methods were explored, finding uncertainties in the attribution of the signal position. However, results were found on the local dissolution of copper under fairly protective (cathodic) thanks to the sensitivity of the SWV-SECM method. Meanwhile, continuous CV recording during SECM mapping allowed a correlation between the degradation rate and the distribution of locally released Cu^{2+}, with surface conductivity and electron donation capacity. The method has not been able to provide information on inhibited surfaces at this stage, but the correlation of the two characteristics opens avenues and methodologies to comprehensively describe and characterize systems of great interest to the industrial and social communities.

CRediT authorship contribution statement

B. Hernández-Concepción: Validation, Formal analysis, Investigation, Data curation, Writing – review & editing, Visualization. **R.M. Souto:** Conceptualization, Resources, Writing – original draft, Writing –

review & editing, Supervision, Project administration, Funding acquisition. **J. Izquierdo:** Methodology, Validation, Formal analysis, Data curation, Writing – original draft, Writing – review & editing, Visualization, Supervision, Funding acquisition.

Declaration of Competing Interest

The authors declare that they have no known competing financial interests or personal relationships that could have appeared to influence the work reported in this paper.

Data availability

Data will be made available on request.

Acknowledgement

Funding by the Spanish Ministry of Science and Innovation (MICINN, Madrid, Spain) and the European Regional Development Fund (Brussels, Belgium) MCIN/AEI/10.13039/501100011033/FEDER,UE under grant PID2021–127445NB-I00 is acknowledged. B.H.-C. acknowledges the collaboration grant awarded by the Spanish Ministry of Education and Professional Training (*Ministerio de Educación y Formación Profesional*). J.I. acknowledges NANOtec, INTech, *Cabildo de Tenerife* and ULL for laboratory facilities.

Supplementary materials

Supplementary material associated with this article can be found, in the online version, at doi:10.1016/j.electacta.2023.143538.

References

[1] J. Kwak, A.J. Bard, Scanning electrochemical microscopy. Theory of the feedback mode, Anal. Chem. 61 (1989) 1221–1227, https://doi.org/10.1021/ac00186a009.
[2] A.J. Bard, G. Denuault, C. Lee, D. Mandler, D.O. Wipf, Scanning electrochemical microscopy: a new technique for the characterization and modification of surfaces, Acc. Chem. Res. 23 (1990) 357–363, https://doi.org/10.1021/ar00179a002.
[3] N.A. Payne, L.I. Stephens, J. Mauzeroll, The application of scanning electrochemical microscopy to corrosion research, Corrosion 73 (2017) 759–780, https://doi.org/10.5006/2354.
[4] M.V. Mirkin, W. Nogala, J. Velmurugan, Y. Wang, Scanning electrochemical microscopy in the 21st century. Update 1: five years after, Phys. Chem. Chem. Phys. 13 (2011) 21196–21212, https://doi.org/10.1039/c1cp22376c.
[5] J.J. Santana, M. Pähler, W. Schuhmann, R.M. Souto, Investigation of copper corrosion inhibition with frequency-dependent alternating-current scanning electrochemical microscopy, Chempluschem 77 (2012) 707–712, https://doi.org/10.1002/cplu.201200091.
[6] J.J. Santana, J. Izquierdo, R.M. Souto, Uses of scanning electrochemical microscopy (SECM) for the characterization with spatial and chemical resolution of thin surface layers and coating systems applied on metals: a review, Coatings 12 (2022) 637, https://doi.org/10.3390/coatings12050637.
[7] K. Mansikkamäki, P. Ahonen, G. Fabricius, L. Murtomäki, K. Kontturi, Inhibitive effect of benzotriazole on copper surfaces studied by SECM, J. Electrochem. Soc. 152 (2005) B12–B16, https://doi.org/10.1149/1.1829413.
[8] K. Mansikkamäki, U. Haapanen, C. Johans, K. Kontturi, M. Valden, Adsorption of benzotriazole on the surface of copper alloys studied by SECM and XPS, J. Electrochem. Soc. 153 (2006) B311–B318, https://doi.org/10.1149/1.2208912.
[9] K. Mansikkamäki, C. Johans, K. Kontturi, The effect of oxygen on the inhibition of copper corrosion with benzotriazole, J. Electrochem. Soc. 153 (2006) B22–B24, https://doi.org/10.1149/1.2130569.
[10] J. Izquierdo, J.J. Santana, S. González, R.M. Souto, Uses of scanning electrochemical microscopy for the characterization of thin inhibitor films on reactive metals: the protection of copper surfaces by benzotriazole, Electrochim. Acta 55 (2010) 8791–8800, https://doi.org/10.1016/j.electacta.2010.08.020.
[11] J. Izquierdo, J.J. Santana, S. González, R.M. Souto, Scanning microelectrochemical characterization of the anti-corrosion performance of inhibitor films formed by 2-mercaptobenzimidazole on copper, Prog. Org. Coatings 74 (2012) 526–533, https://doi.org/10.1016/j.porgcoat.2012.01.019.
[12] S. Varvara, G. Caniglia, J. Izquierdo, R. Bostan, L. Găină, O. Bobis, R.M. Souto, Multiscale electrochemical analysis of the corrosion control of bronze in simulated acid rain by horse-chestnut (Aesculus hippocastanum L.) extract as green inhibitor, Corros. Sci. 165 (2020), 108381, https://doi.org/10.1016/j.corsci.2019.108381.
[13] D.K. Kozlica, B. Hernández-Concepción, J. Izquierdo, R.M. Souto, I. Milošev, In situ, real-time imaging of redox-active species on Al/Cu galvanic couple and corrosion inhibition with 2-mercaptobenzimidazole and octylphosphonic acid, Corros. Sci. 217 (2023), 111114, https://doi.org/10.1016/j.corsci.2023.111114.
[14] Z.J. Barton, J. Rodríguez-López, Fabrication and demonstration of mercury disc-well probes for stripping-based cyclic voltammetry scanning electrochemical microscopy, Anal. Chem. 89 (2017) 2716–2723, https://doi.org/10.1021/acs.analchem.6b04022.
[15] Z.T. Gossage, J. Hui, D. Sarbapalli, J. Rodríguez-López, Coordinated mapping of Li^+ flux and electron transfer reactivity during solid-electrolyte interphase formation at a graphene electrode, Analyst 145 (2020) 2631–2638, https://doi.org/10.1039/c9an02637a.
[16] R.M. Souto, Y. González-García, D. Battistel, S. Daniele, On the use of mercury-coated tips in scanning electrochemical microscopy to investigate galvanic corrosion processes involving zinc and iron, Corros. Sci. 55 (2012) 401–406, https://doi.org/10.1016/j.corsci.2011.11.003.
[17] R.M. Souto, Y. González-García, D. Battistel, S. Daniele, In situ scanning electrochemical microscopy (SECM) detection of metal dissolution during zinc corrosion by means of mercury sphere-cap microelectrode tips, Chem. - A Eur. J. 18 (2012) 230–236, https://doi.org/10.1002/chem.201102325.
[18] M. Janotta, D. Rudolph, A. Kueng, C. Kranz, H.S. Voraberger, W. Waldhauser, B. Mizaikoff, Analysis of corrosion processes at the surface of diamond-like carbon protected zinc selenide waveguides, Langmuir 20 (2004) 8634–8640, https://doi.org/10.1021/la049042h.
[19] D. Rudolph, S. Neuhuber, C. Kranz, M. Taillefert, B. Mizaikoff, Scanning electrochemical microscopy imaging of rhodochrosite dissolution using gold amalgam microelectrodes, Analyst 129 (2004) 443–448, https://doi.org/10.1039/b400051j.
[20] S. Daniele, I. Ciani, M.A. Baldo, C. Bragato, Application of sphere cap mercury microelectrodes and scanning electrochemical microscopy (SECM) for heavy metal monitoring at solid/solution interfaces, Electroanalysis 19 (2007) 2067–2076, https://doi.org/10.1002/elan.200703909.
[21] S.V. Lamaka, O.V. Karavai, A.C. Bastos, M.L. Zheludkevich, M.G.S. Ferreira, Monitoring local spatial distribution of Mg^{2+}, pH and ionic currents, Electrochem. Commun. 10 (2008) 259–262, https://doi.org/10.1016/j.elecom.2007.12.003.
[22] S.V. Lamaka, M.G. Taryba, M.L. Zheludkevich, M.G.S. Ferreira, Novel solid-contact ion-selective microelectrodes for localized potentiometric measurements, Electroanalysis 21 (2009) 2447–2453, https://doi.org/10.1002/elan.200900258.
[23] A.C. Bastos, M.G. Taryba, O.V. Karavai, M.L. Zheludkevich, S.V. Lamaka, M.G. S. Ferreira, Micropotentiometric mapping of local distributions of Zn^{2+} relevant to corrosion studies, Electrochem. Commun. 12 (2010) 394–397, https://doi.org/10.1016/j.elecom.2010.01.002.
[24] R.M.P. da Silva, J. Izquierdo, M.X. Milagre, R.A. Antunes, R.M. Souto, I. Costa, Development of an Al^{3+} ion-selective microelectrode for the potentiometric microelectrochemical monitoring of corrosion sites on 2098−T351 aluminum alloy surfaces, Electrochim. Acta 415 (2022), 140260, https://doi.org/10.1016/j.electacta.2022.140260.
[25] D. Filotás, B.M. Fernández-Pérez, J. Izquierdo, A. Kiss, L. Nagy, G. Nagy, R. M. Souto, Improved potentiometric SECM imaging of galvanic corrosion reactions, Corros. Sci. 129 (2017) 136–145, https://doi.org/10.1016/j.corsci.2017.10.006.
[26] A.P.R.D. Souza, A.S. Lima, M.O. Salles, A.N. Nascimento, M. Bertotti, The use of a gold disc microelectrode for the determination of copper in human sweat, Talanta 83 (2010) 167–170, https://doi.org/10.1016/j.talanta.2010.09.001.
[27] J. Zhuang, L. Zhang, W. Lu, D. Shen, R. Zhu, D. Pan, Determination of trace copper in water samples by anodic stripping voltammetry at gold microelectrode, Int. J. Electrochem. Sci. 6 (2011) 4690–4699.
[28] S. Park, C.S. Maier, D. Koley, Anodic stripping voltammetry on a carbon-based ion-selective electrode, Electrochim. Acta 390 (2021), 138855, https://doi.org/10.1016/j.electacta.2021.138855.
[29] D. Ruhlig, W. Schuhmann, Spatial imaging of Cu^{2+}-ion release by combining alternating current and underpotential stripping mode scanning electrochemical microscopy, Electroanalysis 19 (2007) 191–199, https://doi.org/10.1002/elan.200603693.
[30] A. Papaderakis, A.G. Anastopoulos, S. Sotiropoulos, Electrochemical studies of processes occurring at the polycrystalline Cu electrode/methanol interface, J. Electroanal. Chem. 783 (2016) 217–225, https://doi.org/10.1016/j.jelechem.2016.11.017.
[31] J. Izquierdo, B.M. Fernández-Pérez, A. Eifert, R.M. Souto, C. Kranz, Simultaneous atomic force - scanning electrochemical microscopy (AFM-SECM) imaging of copper dissolution, Electrochim. Acta 201 (2016) 320–332, https://doi.org/10.1016/j.electacta.2015.12.160.
[32] J. Izquierdo, A. Eifert, C. Kranz, R.M. Souto, In situ investigation of copper corrosion in acidic chloride solution using atomic force-scanning electrochemical microscopy, Electrochim. Acta 247 (2017) 588–599, https://doi.org/10.1016/j.electacta.2017.07.042.
[33] Z.J. Barton, J. Rodríguez-López, Cyclic voltammetry probe approach curves with alkali amalgams at mercury sphere-cap scanning electrochemical microscopy probes, Anal. Chem. 89 (2017) 2708–2715, https://doi.org/10.1021/acs.analchem.6b04093.
[34] M.A. Alpuche-Aviles, J.E. Baur, D.O. Wipf, Imaging of metal ion dissolution and electrodeposition by anodic stripping voltammetry-scanning electrochemical microscopy, Anal. Chem. 80 (2008) 3612–3621, https://doi.org/10.1021/ac702568c.
[35] L. Díaz-Ballote, M. Alpuche-Aviles, D.O. Wipf, Fast-scan cyclic voltammetry-scanning electrochemical microscopy, J. Electroanal. Chem. 604 (2007) 17–25, https://doi.org/10.1016/j.jelechem.2007.02.023.

[36] D.S. Schrock, D.O. Wipf, J.E. Baur, Feedback effects in combined fast-scan cyclic voltammetry-scanning electrochemical microscopy, Anal. Chem. 79 (2007) 4931–4941, https://doi.org/10.1021/ac0703911.
[37] D.S. Schrock, J.E. Baur, Chemical imaging with combined fast-scan cyclic voltammetry-scanning electrochemical microscopy, Anal. Chem. 79 (2007) 7053–7061, https://doi.org/10.1021/ac071155t.
[38] P. Salaün, C.M.G. Van Den Berg, Voltammetric detection of mercury and copper in seawater using a gold microwire electrode, Anal. Chem. 78 (2006) 5052–5060, https://doi.org/10.1021/ac060231+.
[39] P. Salaün, B. Planer-Friedrich, C.M.G. van den Berg, Inorganic arsenic speciation in water and seawater by anodic stripping voltammetry with a gold microelectrode, Anal. Chim. Acta 585 (2007) 312–322, https://doi.org/10.1016/j.aca.2006.12.048.
[40] C.S. Chapman, C.M.G. Van Den Berg, Anodic stripping voltammetry using a vibrating electrode, Electroanalysis 19 (2007) 1347–1355, https://doi.org/10.1002/elan.200703873.
[41] G.M.S. Alves, J.M.C.S. Magalhães, P. Salaün, C.M.G. van den Berg, H.M.V. M. Soares, Simultaneous electrochemical determination of arsenic, copper, lead and mercury in unpolluted fresh waters using a vibrating gold microwire electrode, Anal. Chim. Acta 703 (2011) 1–7, https://doi.org/10.1016/j.aca.2011.07.022.
[42] C. Garnier, L. Lesven, G. Billon, A. Magnier, O. Mikkelsen, I. Pižeta, Voltammetric procedure for trace metal analysis in polluted natural waters using homemade bare gold-disk microelectrodes, Anal. Bioanal. Chem. 386 (2006) 313–323, https://doi.org/10.1007/s00216-006-0625-9.
[43] G.T. Burstein, C. Liu, R.M. Souto, S.P. Vines, Origins of pitting corrosion, Corros. Eng. Sci. Technol. 39 (2004) 25–30, https://doi.org/10.1179/147842204225016859.
[44] G.T. Burstein, C. Liu, R.M. Souto, The effect of temperature on the nucleation of corrosion pits on titanium in Ringer's physiological solution, Biomaterials 26 (2005) 245–256, https://doi.org/10.1016/j.biomaterials.2004.02.023.
[45] P. Dauphin-Ducharme, R.M. Asmussen, D.W. Shoesmith, J. Mauzeroll, In-situ Mg^{2+} release monitored during magnesium alloy corrosion, J. Electroanal. Chem. 736 (2015) 61–68, https://doi.org/10.1016/j.jelechem.2014.10.030.
[46] S.H. Salleh, N. Birbilis, M. Musameh, K. Venkatesan, S. Thomas, On the Development and application of an in-house Fabricated Mg^{2+} ion selective microelectrode (ISME) for assessing Mg corrosion, J. Electrochem. Soc. 165 (2018) C771–C776, https://doi.org/10.1149/2.0591811jes.
[47] U.K. Sur, F. Marken, R.G. Compton, B.A. Coles, Microwave effects on the electrochemical deposition of copper, New J. Chem. 28 (2004) 1544–1549, https://doi.org/10.1039/b411536h.
[48] S. Daniele, M.J. Pena, Cyclic voltammetric investigation of the Cu-histidine system at platinum conventional and microelectrodes, Electrochim. Acta 38 (1993) 165–174, https://doi.org/10.1016/0013-4686(93)85125-I.
[49] M. Donnici, M.A. Baldo, S. Daniele, An electrochemical study on the interaction between copper ions and the eco-friendly corrosion inhibitor decanoic acid in a 50% (v/v) ethanol/water mixture, J. Mol. Liq. 332 (2021), 115829, https://doi.org/10.1016/j.molliq.2021.115829.
[50] M. Zhou, N. Myung, X. Chen, K. Rajeshwar, Electrochemical deposition and stripping of copper, nickel and copper nickel alloy thin films at a polycrystalline gold surface: a combined voltammetry-coulometry-electrochemical quartz crystal microgravimetry study, J. Electroanal. Chem. 398 (1995) 5–12, https://doi.org/10.1016/0022-0728(95)04001-0.
[51] Y. Bonfil, M. Brand, E. Kirowa-Eisner, Determination of sub-μg l^{-1} concentrations of copper by anodic stripping voltammetry at the gold electrode, Anal. Chim. Acta 387 (1999) 85–95, https://doi.org/10.1016/S0003-2670(99)00066-5.
[52] D. Krznarić, T. Goričnik, Reactions of copper on the Au(111) surface in the underpotential deposition region from chloride solutions, Langmuir 17 (2001) 4347–4351, https://doi.org/10.1021/la001562z.
[53] P. Westbroek, F. Twagiramungu, J. De Strycker, I. Vanmoortel, E. Temmerman, Voltammetric measurement of [Cu(II)]/[Cu(I)] at a platinum rotating disc electrode and control by electrolysis at a platinum net electrode in chloride solutions, Anal. Lett. 33 (2000) 2243–2258, https://doi.org/10.1080/00032710008543186.
[54] J. Xia, W. Wei, Y. Hu, H. Tao, L. Wu, A novel voltammetric method for the direct determination of copper in complex environmental samples, Anal. Sci. 20 (2004) 1037–1041, https://doi.org/10.2116/analsci.20.1037.
[55] G. Herzog, D.W.M. Arrigan, Determination of trace metals by underpotential deposition-stripping voltammetry at solid electrodes, TrAC - Trends Anal. Chem. 24 (2005) 208–217, https://doi.org/10.1016/j.trac.2004.11.014.
[56] J. Wang, E. Sucman, B. Tian, Stripping potentiometric measurements of copper in blood using gold microelectrodes, Anal. Chim. Acta 286 (1994) 189–195, https://doi.org/10.1016/0003-2670(94)80159-2.
[57] B. Hernández-Concepción, R.M. Souto, J. Izquierdo, Evaluation of the applicability of voltammetric modes in Scanning Electrochemical Microscopy for the in situ characterization of the corrosion of copper-based materials, Metals (Basel) under review.
[58] G. Sanna, M.I. Pilo, P.C. Piu, N. Spano, A. Tapparo, R. Seeber, Microelectrodes for the determination of heavy metal traces in physiological conditions. Hg, Cu and Zn ions in synthetic saliva, Electroanalysis 14 (2002) 1512–1520, https://doi.org/10.1002/1521-4109(200211)14:21<1512::AID−ELAN1512>3.0.CO;2-3.
[59] H. Shen, J.E. Mark, C.J. Seliskar, H.B. Mark, W.R. Heineman, Stripping voltammetry of copper and lead using gold electrodes modified with self-assembled monolayers, J. Solid State Electrochem. 1 (1997) 241–247, https://doi.org/10.1007/s100080050055.
[60] C. Lefrou, R. Cornut, Analytical expressions for quantitative scanning electrochemical microscopy (SECM), ChemPhysChem 11 (2010) 547–556, https://doi.org/10.1002/cphc.200900600.
[61] T. Chang, C. Leygraf, I.O. Wallinder, Y. Jin, Understanding the barrier layer formed via adding BTAH in copper film electrodeposition, J. Electrochem. Soc. 166 (2019) D10–D20, https://doi.org/10.1149/2.0041902jes.
[62] D. Tromans, R. Sun, Anodic polarization behavior of copper in aqueous chloride/benzotriazole solutions, J. Power Sources. 138 (1991), https://doi.org/10.1016/S0378-7753(01)00555-9, 3235–3224.